Electrodialysis and Nitrate Reduction to Enable Distributed Ammonia Manufacturing from Wastewaters

Jinyu Guo,[†] Matthew J. Liu,[†] Chloe Laguna,[†] Dean M. Miller,[†] Kindle S. Williams,[†] Brandon D. Clark,[†] Carolina Muñoz,[†] Sarah J. Blair,[†] Adam C. Nielander,[‡] Thomas F. Jaramillo,[†,‡] William A. Tarpeh[†,‡,*]

†Department of Chemical Engineering, Stanford University, Stanford, CA, 94305, USA

‡ SUNCAT Center for Interface Science and Catalysis, SLAC National Accelerator Laboratory, Menlo Park, CA, USA

*Corresponding author, Email: wtarpeh@stanford.edu Address: 443 Via Ortega, Room 387, Stanford, CA, 94305, USA. Telephone: 650-497-1324

ABSTRACT

Underutilized wastewaters containing dilute levels of reactive nitrogen (Nr) can help rebalance the nitrogen cycle. This study describes electrodialysis and nitrate reduction (EDNR), a reactive electrochemical separation architecture that combines catalysis and separations to remediate nitrate and ammonium-polluted wastewaters while recovering ammonia. By engineering operating parameters (e.g., background electrolyte, applied potential, electrolyte flow rate), we achieved near-complete recovery and conversion of Nr in both simulated and real wastewaters. EDNR process demonstrated long-term robustness and recovered >100 mM ammonium fertilizer solution from 8.2 mM Nr-containing agricultural runoff. EDNR is the first reported process to our knowledge that remediates dilute real wastewater and recovers ammonia from multiple Nr pollutants, with an energy consumption (245 MJ/kg NH_3-N in simulated wastewater, 920 MJ/kg NH_3-N in agricultural runoff) on par with the state-of-the-art. Demonstrated first at proof-of-

concept and engineered to technology readiness level (TRL) 5, EDNR shows great promise for distributed wastewater treatment and sustainable ammonia manufacturing.

KEYWORDS: electrochemical nitrate reduction reaction, reaction engineering, reactive separation, sustainable ammonia production, wastewater refining

INTRODUCTION

The nitrogen cycle is in urgent need of re-engineering. Nitrogen (N) pollution is widespread — the U.S. Environmental Protection Agency considers it "one of the costliest, most difficult environmental problems we face in the 21st century.[1]" Much of this pollution arises from Haber-Bosch ammonia synthesis, a promising solution to an early 20th century challenge: producing enough fertilizer to feed a growing global population. Despite successfully supplying sufficient fertilizer, the Haber-Bosch process introduced several sustainability challenges due to its use of fossil fuels to synthesize ammonia (NH_3) from inert N_2 at ~700 K and ~100 atm; these extreme conditions require 1-2% of global energy consumption and 1.2% of greenhouse gas emissions.[2–5] In contrast, anthropogenic removal of reactive nitrogen (Nr) from the environment (often as N_2) is only half the rate of its production, leading to costly Nr pollution that has exceeded critical thresholds for environment and human welfare and caused direct damages worth 0.3–3% of annual global gross domestic product.[6,7] Even with universal adoption of known Nr mitigation actions (e.g., efficient fertilizer application and livestock management), environmental discharges of Nr are projected to surpass 95 million tons per year in 2050.[3,7] This perilous gap between Nr production and mitigation calls for transformative technologies that can produce Nr products with low associated emissions and that can remove Nr from the environment.

Instead of solely targeting sustainable Nr production (N_2 to Nr, e.g., electrified ammonia synthesis) or Nr removal (Nr to N_2, e.g., denitrification), we shortcut the inert N_2 intermediate and directly convert Nr pollutants to Nr products through wastewater refining.[8] Globally, wastewater contains a yearly stream of 35–78 million tons Nr, which could offset 15–34% of total Nr required by 2050.[8] Specifically, we target municipal wastewater and agricultural runoff because they contribute over

90% of Nr emissions and often occur in areas where clean water and fertilizer are most needed.[7,8] Among various Nr pollutants, we focus on nitrate (NO_3^-) and ammonium (NH_4^+) because they dominate aqueous Nr pollution, often coexist in target wastewaters, and threaten the health of both ecosystems (e.g., eutrophication) and humans (e.g., methemoglobinemia, colon cancer).[9–12] By targeting both NO_3^- and NH_4^+, we avoid the Nr cascade problem, where Nr species interconvert to continue harming the environment.[4,13] Out of several possible Nr products we leverage the electrochemical nitrate reduction reaction (NO_3RR) to convert nitrate into ammonia, a common fertilizer and chemical precursor. We pursue electrochemical methods because they facilitate replacement of fossil fuels with renewable energy inputs and enable distributed implementation that matches the distributed nature of our target wastewaters. Ultimately, electrochemically refining wastewater NO_3^- and NH_4^+ to NH_3 can (1) remediate legacy Nr pollution in the environment, (2) recover valuable Nr resources, and (3) reduce the need for virgin Nr production and related emissions from Haber-Bosch facilities.

Achieving the full potential of wastewater Nr refining requires overcoming challenges intrinsic to decentralized wastewater feedstocks, including dilute mixed Nr pollutants (typically below 10 mM), low total ionic conductivity, and complex and variable background matrices. In contrast, electrochemical NH_3 recovery and NO_3RR systems are often demonstrated with simplistic matrices with a single Nr species at higher concentrations (usually above 10 mM), well-controlled pH, and high ionic conductivity to operate efficiently. This mismatch in decentralized wastewater characteristics and electrochemical Nr recovery system requirements leads to low efficiency when real wastewater is directly used as the electrolyte. Therefore, we leverage electrochemical reactive separations, where separation and reaction are collated within the same reactor and happen in

tandem.[8,13,14] Unlike processes with discrete reactant separation and catalysis steps, reactive separations utilize separations to create favorable and stable reaction environments from complex feedstocks, and reactions to produce product mixtures that inform separations. Electrochemical reactive separations have been demonstrated to recover carbon (reactive carbon capture),[15–19] sulfur,[20–24] and lithium,[25–30] but have rarely been used to recover NH_3 from NH_4^+-containing[31–33] and from NO_3^--containing[34–37] wastewaters, and even more rarely for wastewaters containing both NH_4^+ and NO_3^-.

In this study, we developed a novel electrochemical reactive separation unit process, Electrodialysis and Nitrate Reduction (EDNR), to recover and synthesize NH_3 from dilute NH_4^+ and NO_3^--polluted wastewaters. EDNR consists of three sub-unit processes: (1) electrodialysis to separate influent NH_4^+ and NO_3^- from wastewater, (2) deprotonation of NH_4^+ with electrochemically *in situ* generated OH^- to recover NH_3, and (3) electrocatalytic reduction of NO_3^- to synthesize NH_3 using polycrystalline titanium (Ti) foil electrodes. This unit process is the first to our knowledge that targets multiple Nr pollutants and recovers NH_3 from both dilute wastewater NH_4^+ and NO_3^- using electrochemical reactive separations. We achieved near-complete Nr conversion and recovery in simulated wastewater through engineering operating parameters. Furthermore, we systematically studied effects of feedstock compositions and tested real wastewaters that span two orders of magnitude in total ionic concentration (well water, agricultural runoff, reverse osmosis retentate). The EDNR process showed excellent stability over 60-hour operation and recovered 12-fold concentrated ready-to-apply NH_3 fertilizer solution from agricultural runoff, with an energy consumption (920 MJ/kg NH_3-N) on par with the state-of-the-art (18–101 MJ/kg NH_3-N from NH_4^+ and 168–31400 MJ/kg NH_3-N from NO_3^-). Our efforts

advanced beyond proof-of-concept to achieve TRL 5 (validation in a relevant environment, i.e., real wastewater), demonstrating that EDNR can be implemented as an individual module or part of a treatment train to enable integrated distributed water treatment and sustainable NH_3 production.

METHODS

Electrodialysis and nitrate reduction (EDNR) reactor and operation

The EDNR reactor is a three-chamber cell, with an anion exchange membrane (AEM, **Table 1**) separating the NH_3 synthesis (left) and influent (middle) chambers, and a cation exchange membrane (CEM, CMI-7000, Membranes International) separating the influent (middle) and NH_3 recovery (right) chambers (**Fig. 1a**). All three chambers have the dimensions: 3.15 cm (H) x 1.8 cm (W) x 1.19 cm (D) (**Fig. S1** in the **Supporting Information, SI**). Semi-batch mode was used, and electrolytes were recirculated between the electrochemical reactor chambers and their corresponding electrolyte reservoirs (total electrolyte volume of 50 mL for each chamber) using peristaltic pumps.

The EDNR process operates in two stages, referred to as the electrodialysis (ED) stage and the nitrate reduction (NR) stage (**Fig. S2–3**). In each ED stage, controlled current is applied to IrO_2-Ta_2O_5/Ti mesh electrode (anode) in the NH_3 synthesis chamber and platinum electrode (cathode) in the NH_3 recovery chamber. Influent NO_3^- and NH_4^+ are separated *via* electromigration into the NH_3 synthesis and NH_3 recovery chambers, respectively; NH_4^+ combines with the electrochemically-generated OH^-, and NH_3 is recovered in the NH_3 recovery chamber ($NH_4^+ + OH^- \rightarrow NH_3 + H_2O$). In each NR stage, controlled potential is applied to the Ti electrode (cathode)

in the NH_3 synthesis chamber and IrO_2-Ta_2O_5/Ti mesh electrode (anode) in the influent chamber; NH_3 is synthesized from the electrochemical NO_3RR ($NO_3^- + 8e^- + 9H^+ \rightarrow NH_3 + 3H_2O$) in the NH_3 synthesis chamber. The two consecutive stages complete one EDNR cycle, and multiple cycles can be conducted to achieve treatment goals (e.g., complete removal and recovery of influent Nr).

Detailed experimental descriptions (e.g., reagents, instrumentation, procedures) are given in **SI Section S1.1** and **S1.2**. Reactor schematics and operation procedures of two-chamber NR reactor, long-term EDNR, and membrane stripping experiments are described in **SI Section S1.3** and **S1.4**. Electrolyte compositions and operating parameters used in all EDNR experiments are summarized in **Table S1**.

Product analysis and key performance metrics

Electrolyte aliquots from all three electrolyte reservoirs were sampled for pH measurement and aqueous product analysis before and after each stage (ED or NR). Due to acid–base equilibria, we reported the sum concentrations of weak conjugate acid–base pairs using nitrite (NO_2^-) to represent the sum of anionic nitrite and nitrous acid (pKa 3.16 at 25 °C), and ammonia (NH_3) to represent the sum of cationic ammonium (pKa 9.25 at 25 °C) and ammonia for brevity. NO_3^- and NO_2^- concentrations were quantified using anion chromatography, and NH_3 concentrations were quantified using spectrophotometric flow injection analysis. See **SI Section S1.5** for detailed sample analysis methods.

To evaluate efficiency of the EDNR process in recovering NH_3 from influent Nr, we defined the following two metrics:

NH_3 recovery efficiency (η_{Recovery}):

$$\eta_{\text{Recovery, Cycle } i} = \frac{[NH_3]_{\text{Rec, ED}i} - [NH_3]_{\text{Rec, Ini}}}{[NH_3]_{\text{Inf, Ini}}} \qquad \textbf{Eqn. 1}$$

Where $[NH_3]_{\text{Rec, ED}i}$ is the NH_3 concentration in the NH_3 recovery chamber at the end of the ED stage in cycle i, $[NH_3]_{\text{Rec, Ini}}$ is the initial NH_3 concentration in the NH_3 recovery chamber before EDNR starts (i.e., in the initial wastewater), and $[NH_3]_{\text{Inf, Ini}}$ is the initial NH_3 concentration in the influent chamber before EDNR starts.

NH_3 synthesis efficiency ($\eta_{\text{Synthesis}}$):

$$\eta_{\text{Synthesis, Cycle } i} = \frac{[NH_3]_{\text{Syn, NR}i} - [NH_3]_{\text{Syn, Ini}}}{[NO_3^-]_{\text{Inf, Ini}}} \qquad \textbf{Eqn. 2}$$

where $[NH_3]_{\text{Syn, NR}i}$ is the NH_3 concentration in the NH_3 synthesis chamber at the end of the NR stage in cycle i, $[NH_3]_{\text{Syn, Ini}}$ is the initial NH_3 concentration in the NH_3 synthesis chamber before EDNR starts, and $[NO_3^-]_{\text{Inf, Ini}}$ is the initial NO_3^- concentration in the influent before EDNR starts.

Definitions of the other performance metrics for the ED stage (NH_4^+ and NO_3^- ED current efficiency, and NO_3^- ED flux) and NR stage (total current density, NH_3 partial current density, time-averaged NR NO_3^- removal rate, Faradaic efficiency) are defined in **SI Section S1.7**. All current densities shown were calculated using the electrode geometric area.

RESULTS AND DISCUSSION

Proof-of-concept EDNR

As proof-of-concept, we used simulated wastewater with relatively simple compositions and intermediate Nr concentrations between high values used in typical fundamental research (**Fig. S6**) and our target wastewater feedstocks as the EDNR influent (13.9 mM $(NH_4)_2SO_4$ + 1.6 mM KNO_3). During ED stages, influent NH_4^+ and NO_3^- were separated into the NH_3 recovery and NH_3 synthesis chambers, respectively (**Fig. 1b**), and favorable pH environments were achieved by electrochemical water oxidation and reduction reactions: pH >9 in the NH_3 recovery chamber to recover NH_4^+ as NH_3, and pH <3 in the NH_3 synthesis chamber to prepare for NR. Ti was chosen as a generic NO_3RR electrocatalyst because it is selective to NH_3, abundant, and corrosion resistant, all of which are suitable characteristics for treating real wastewater.[38–40] Ti also exhibits higher nitrate reduction activity in acidic environments, making it well-suited for EDNR.[38,40] In the following NR stages, NH_3 was synthesized from Ti-catalyzed reduction of the electromigrated NO_3^-. By repeating the ED and NR stages for multiple cycles, we removed increasing amounts of NH_4^+ and NO_3^- from the influent. At the end of three EDNR cycles, >70% of influent NH_4^+ was recovered (defined as NH_3 recovery efficiency, η_{Recovery}, **Eqn. 1**), and 25% of influent NO_3^- was converted to NH_3 (defined as NH_3 synthesis efficiency, $\eta_{\text{Synthesis}}$, **Eqn. 2**). The total nitrogen balance in the system was also very well closed (–11.2% to +1.3% among all stages, **Fig. S8d**). Although the process functioned as designed, $\eta_{\text{Synthesis}}$ was consistently lower than η_{Recovery}, indicating more complete recovery from NH_4^+ than conversion from NO_3^- despite the much higher influent NH_4^+ concentration. The poor $\eta_{\text{Synthesis}}$ resulted from low NO_3RR activity and NH_3

184 selectivity (**Fig. S12**), which necessitates improving the NR process to extract NH_3 more

185 completely from wastewater Nr (especially wastewaters with high NO_3^- concentrations).

186

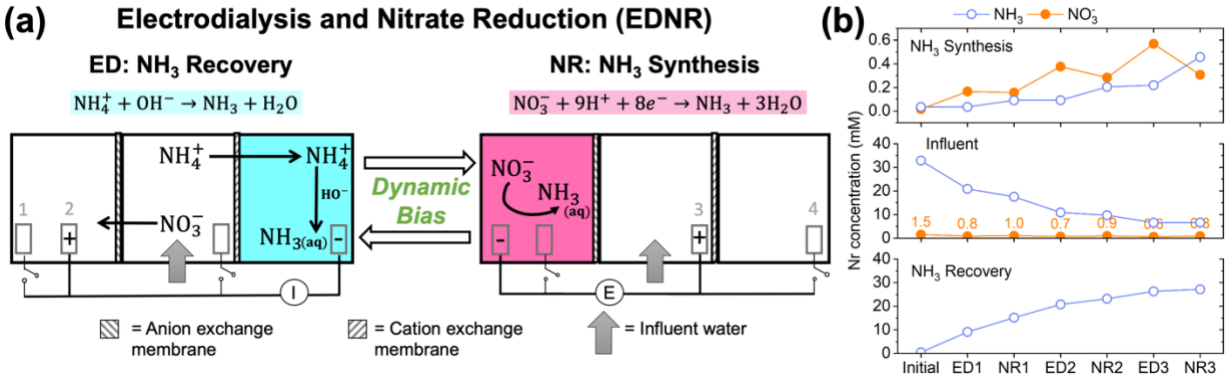

187

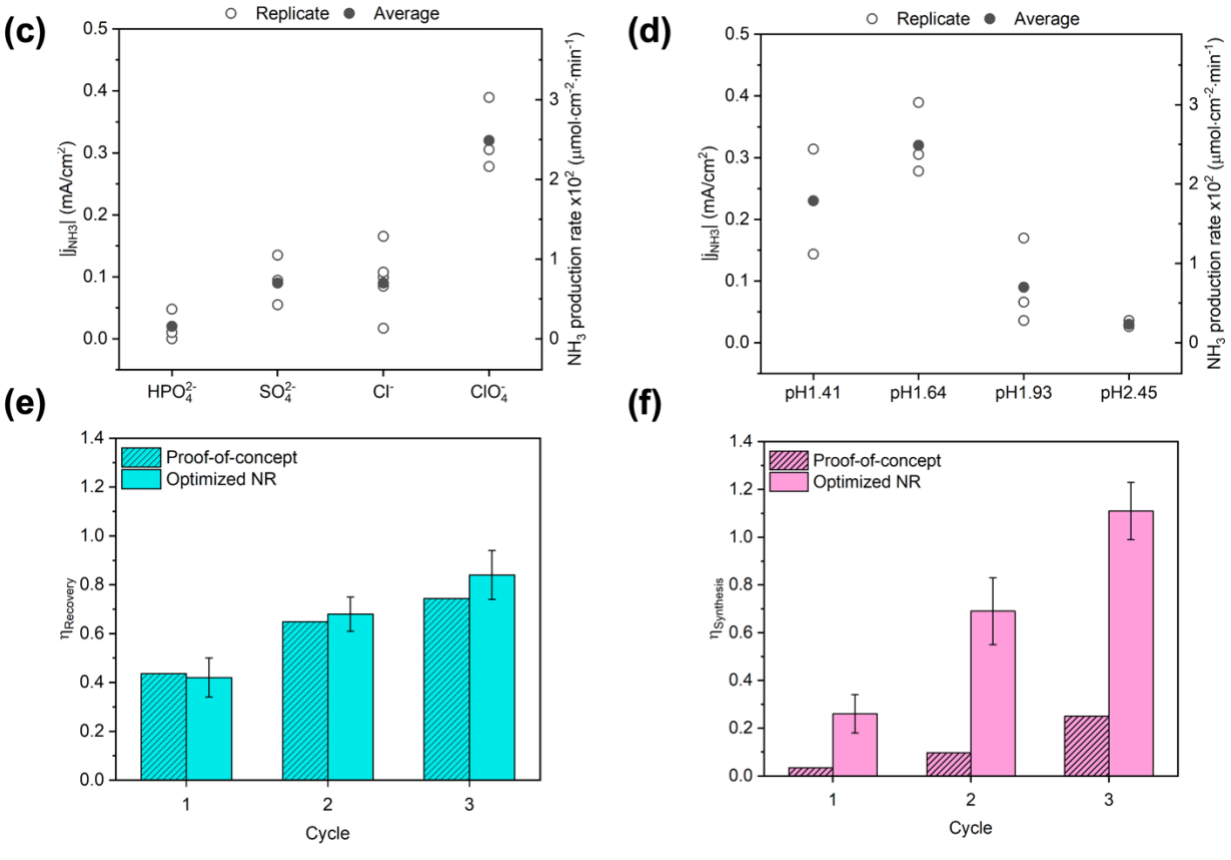

188

Fig. 1 (a) Schematics of the EDNR process. Electrode 1: Ti foil, 2 and 3: IrO_2-Ta_2O_5/Ti mesh, 4: Pt foil. I and E represent controlled applied current and potential in ED and NR stages, respectively. **(b)** Trends of NH_3 and NO_3^- concentrations in proof-of-concept experiment. NO_3^- concentrations in the influent chamber are enumerated to highlight their values on the large scale used for NH_3 concentrations. **(c)** Magnitude of NH_3 partial current density (left y-axis) and production rate (right y-axis) in background electrolytes with a variety of anions: 0.5 M Na_2HPO_4, 0.5 M Na_2SO_4, 1 M NaCl, and 1 M $NaClO_4$, pH adjusted to 1.72 with 2 M $HClO_4$. **(d)** Magnitude of NH_3 partial current density (left y-axis) and production rate (right y-axis) in 1 M $NaClO_4$ with a variety of initial pH: 1.41, 1.64, 1.93, and 2.45. All experiments in (c) and (d) were conducted in two-chamber reactors, 10 mL specified background electrolyte was added to both chambers, and 10 mM $NaNO_3$ was added to the cathode chamber. Applied static potential of –0.8 V vs. RHE for 30 min. Open symbols represent results from each replicate experiment, and filled symbols represent the average values. Comparison of **(e)** NH_3 recovery and **(f)** NH_3 synthesis efficiencies in proof-of-concept and optimized NR experiments. Error bars represent ± one standard deviation.

Engineering of EDNR operating parameters

The EDNR process leverages several key operating parameters (e.g., background electrolyte, applied current/potential, stage duration, electrolyte flow rate) that enable flexible tuning of this process to adapt to treatment goals. To improve the low $\eta_{\text{Synthesis}}$ in proof-of-concept experiments, we employed electrolyte engineering, which has been shown to substantially influence the activity and selectivity of electrocatalytic reactions[41–44] including NO_3RR.[38,45,46] Rather than directly conducting NO_3RR in complex, dynamic decentralized wastewaters, the EDNR reactor separates the NH_3 synthesis chamber from the influent using an AEM. This design allows for flexible selection of background electrolyte, as well as conditioning of the NR electrolyte through preceding ED stages. Although high concentration of background electrolyte[40] and acidic pH[38,40]

213 are known to enhance NO_3RR activity and NH_3 selectivity on Ti, effects of anion identity and
214 specific optimal pH are not well understood. To address this knowledge gap, we varied the NR
215 background electrolyte anion identity and initial pH in an isolated two-chamber reactor to identify
216 the optimal NR environment (see **SI Section S1.3**). The background electrolyte concentration was
217 fixed as 1 M (cation concentration) to ensure high NO_3RR activity,[34,40] and the cation identity was
218 fixed as Na^+. First, we found that weakly adsorbing ClO_4^- [9,46,47] outperformed other anions
219 commonly used in electrocatalysis studies and present in wastewater (HPO_4^{2-}, SO_4^{2-} and Cl^-) and
220 exhibited the highest NH_3 partial current density (j_{NH_3}, **Fig. 1c**). Second, the highest j_{NH_3} occurred
221 in an optimal initial pH around 1.6 (**Fig. 1d**), above which Ti electrode shows little activity (total
222 current density j_{total} <0.2 mA/cm^2, **Fig. S9b**) and below which hydrogen evolution reaction (HER)
223 and Ti hydride formation[39] dominate electrode reactions (>50% FE, **Fig. S9d**). In addition to
224 electrolyte engineering, we previously found that changing the applied potential pattern from static
225 to pulsed can periodically replenish the local electrolyte acidity and increase the ammonia-to-
226 nitrite selectivity.[40] When we applied a pulsed potential to this two-chamber system, j_{NH_3} doubled
227 (**Fig. S10**).

228

229 Therefore, we engineered the following EDNR operating parameters to enhance NR performance
230 (**Table 1**): (1) chose 1 M $NaClO_4$ as the NH_3 synthesis chamber background electrolyte to
231 maximize NH_3 partial current density, (2) used a monovalent-selective AEM to limit the
232 disturbance in NR activity from multivalent and strongly adsorbing anions in wastewater, (3)
233 increased ED stage applied current to achieve optimal initial bulk pH for subsequent NR stages,
234 (4) applied pulsed potential (reduction potential of –0.8 V vs. RHE) in NR stages to enhance NH_3

selectivity, and (5) increased NR stage electrolyte flow rate to accelerate nitrate removal.[40] We conducted triplicate 3-cycle EDNR experiments using the same simulated wastewater (13.9 mM $(NH_4)_2SO_4$ + 1.61 mM KNO_3) as the influent; the set of experiments is referred to as optimized NR in the following text. Compared to proof-of-concept, we successfully increased the FE_{NH_3} by 1.2–2.9 times (to around 20%) and j_{NH_3} by 6–14 times (to –0.6 to –1.2 mA/cm^2, **Fig. S12**). Although FE_{NH_3} and j_{NH_3} observed in optimized NR are lower than values reported in the NO_3RR literature,[9] we note that they were achieved in realistically dilute NO_3^- concentration and could be improved when using higher NO_3^- feedstocks.[38,40] FE_{NH_3} and j_{NH_3} remained steady across all cycles, which we attribute to ED repeatedly accessing a favorable NH_3 synthesis chamber pH for NR. Importantly, optimized NR closed the gap between NH_3 synthesis and NH_3 recovery by achieving near-unity efficiency for both metrics at the end of 3 cycles from the same simulated wastewater influent (0.84±0.10 for $\eta_{Recovery}$, and 1.11±0.12 for $\eta_{Synthesis}$, **Fig. 1e–f**).

Table 1 Comparison of experiment conditions used in proof-of-concept and optimized NR

	Proof-of-concept	**Optimized NR**
Influent	13.9 mM $(NH_4)_2SO_4$ + 1.61 mM KNO_3	
NR electrolyte	0.1 M $KClO_4$	1 M $NaClO_4$
AEM	General (AMI-700)	Monovalent-selective (Selemion AMVN)
ED current density	2.63 mA/cm^2	3.95 mA/cm^2
ED duration	60 min	
NR potential	–0.6 V vs. RHE, potentiostatic	–0.8 V vs. RHE, pulsed (10 s at reduction potential, followed by 10 s at open circuit)
NR flow rate	30 mL/min	100 mL/min
NR duration	120 min	

Next, we examined ED performance after implementing NR reaction environment engineering. Near-complete removal (**Eqn. S8–9**) was achieved for both NH_4^+ (87%) and NO_3^- (84%) at the end of 3 cycles. But unlike the steady NR performance, the ED performance decayed as more Nr was removed from the influent: current efficiency for NH_4^+ dropped from 57% (ED1) to 25% (ED3), and from 4.5% (ED1) to 1.0% (ED3) for NO_3^- (proportional to ionic flux, **Fig. S13a, S14a**). We identified that (1) the ED ionic fluxes were likely controlled by transport from the influent to AEM/CEM, rather than transport across the membranes, and (2) the decreasing transport from the influent to AEM/CEM originated from the decreasing influent Nr concentrations (see **SI Section S3.2.2**). Within the same cycle, the substantial difference in current efficiency between NH_4^+ and NO_3^- was caused by their abundance and conductivity relative to coexisting ions (transference number) in the influent. In the simulated wastewater NH_4^+ has an initial transference number of 0.95 and was the major charge-carrying cation across the CEM, whereas NO_3^- has an initial transference number of 0.025 due to its low concentration and was a minor charge-carrying anion across the AEM (see **SI Section S2**). Compared to proof-of-concept, NO_3^- ED flux was improved by 0.4–3.7 times in optimized NR, confirming that the monovalent-selective AEM exhibits favorable selectivity towards NO_3^- (**Fig. S13b, S14b**).

To enhance ED performance, we first tried shortening the ED duration to avoid operating under low transport driving force (low influent Nr concentrations, see **SI Section S3.2.3**). We found that halving the ED duration (i.e., halving the total charge passed, 30 min in ED2 and ED3) did not significantly impact the current efficiency nor flux for NH_4^+ and NO_3^- transport but lowered $\eta_{Recovery}$ (**Fig. S15**). The shortened ED duration also led to higher than optimal pH in the NH_3

synthesis chamber and consequently impaired $\eta_{\text{Synthesis}}$ (**Fig. S16**). The unexpected adverse effects of shortened ED duration exhibited on NR performance underscore the intimate connection between separation and reaction in EDNR: separation influences subsequent reaction by conditioning the reaction environment. Aside from shortening ED duration, we tried enhancing transport by increasing the electrolyte flow rate during the shortened ED stages (to the same flow rate as in NR, 100 mL/min). The higher electrolyte flow rate helped restore a high η_{Recovery}, but the NH_3 synthesis chamber pH was not significantly altered, and $\eta_{\text{Synthesis}}$ remained low (**Fig. S15–16**). Therefore, we concluded that while the combination of shortened ED stage duration (less charge passed) and high electrolyte flow rate could generate high η_{Recovery}, sufficient ED stage duration is critical to achieving the optimal NR reaction environment and associated high $\eta_{\text{Synthesis}}$. In the following experiments, operating parameters from optimized NR were applied unless otherwise specified.

Impacts of influent compositions on EDNR performance

As the target feedstocks for EDNR, decentralized wastewaters exhibit a wide range of compositions dependent on the source location and time;[10,48–50] however, feedstock composition impacts have rarely been studied in electrochemical Nr conversion and recovery literature. We have demonstrated that NO_3RR is particularly prone to background electrolyte composition and initial pH. To further inform high-TRL EDNR implementation, we systematically studied influent composition effects on the unit process level using increasingly realistic feedstocks. First, we deconvoluted effects of common wastewater components by independently introducing them to the simulated wastewater matrix used in proof-of-concept and optimized NR via three modified

simulated wastewaters: NO_3^--laden, SO_4^{2-}-laden, and Cl^--laden. Then, we moved on to using three real wastewater feedstocks: well water (Stanford, CA), agricultural runoff (Salinas, CA), and reverse osmosis (RO) retentate (from full advanced treatment of municipal wastewater, Silicon Valley Clean Water, Redwood City, CA) (**Fig. 2a**). In the following discussion, we (1) analyze impacts of each scenario on NH_3 synthesis, (2) discuss generalizable implications of each scenario on NH_3 recovery, and (3) identify strategies for EDNR to adapt to different feedstock compositions.

Modified simulated wastewaters

To imitate NO_3^- concentrations in different feedstocks (e.g., 20–60 mM in reverse osmosis retentate[50,51]), we used NO_3^--laden simulated wastewater as EDNR influent (13.9 mM $(NH_4)_2SO_4$ + 26.4 mM KNO_3). Compared to using the baseline simulated wastewater (optimized NR), both the NO_3^- ED flux and concentration in the NH_3 synthesis chamber increased nearly 1-to-1 with the increase in influent NO_3^- concentration (**Fig. S17a–b**). During NR, j_{total} was not significantly different (**Fig. S17c**), but FE_{NH_3} improved to >40%, and j_{NH_3} increased by 1.9–2.5 times (**Fig. 2b** and **Fig. S17d–e**). Unlike NO_3^- ED flux, j_{NH_3} did not increase linearly with NO_3^- concentration, suggesting a fractional reaction rate order with respect to NO_3^-;[52] the enhanced $FE_{NO_2^-}$ indicated that further hydrogenation of NO_2^- to NH_3 was also limited (e.g., by insufficient proton supply). [40] Despite the higher j_{NH_3}, end-of-run $\eta_{Synthesis}$ decreased from 1.11 ± 0.12 in baseline simulated wastewater to 0.11 as a result of incomplete conversion of influent NO_3^- (**Fig. 2c** and **Fig. S18a**). Therefore, achieving a high $\eta_{Synthesis}$ in NO_3^--rich feedstocks requires longer NR stage duration, more EDNR operation cycles, or more active NR electrodes.

Beyond NO_3^-, we introduced SO_4^{2-} and Cl^- because they are the most common divalent and monovalent anions in wastewaters. We added high concentrations to the baseline simulated wastewater (13.9 mM $(NH_4)_2SO_4$ + 1.6 mM KNO_3 + 50 mM Na_2SO_4 or 100 mM NaCl) as the influent to amplify their effects. Amidst these concentrated coexisting anions, NO_3^- transference number decreased by an order of magnitude (**SI Section S2**). The NO_3^- ED flux in both scenarios was lowered significantly in cycle 1, but gradually converged towards optimized NR, leading to similar NO_3^- concentrations in the NH_3 synthesis chamber starting from cycle 2 (**Fig. S19a–b**). The monovalent-selective AEM largely blocked SO_4^{2-} from entering the NH_3 synthesis chamber in the SO_4^{2-}-laden scenario, and selectively transported Cl^- to maintain charge neutrality in the Cl^--laden scenario (**Fig.S19c–f**). As shown in NO_3RR electrolyte engineering experiments, additional SO_4^{2-} and Cl^- suppressed FE_{NH_3} and lowered j_{NH_3} (**Fig. 2b**). In the Cl^--laden scenario, the insufficient acidity at the beginning of each NR stage (caused by chlorine evolution reaction during ED, **Fig. S20b**) further impaired NR performance. Consequently, end-of-run $\eta_{Synthesis}$ decreased from 1.11 ± 0.12 in baseline simulated wastewater to 0.32 and 0.03 in SO_4^{2-}-laden and Cl^--laden scenarios, respectively (**Fig. 2b** and **Fig. S18a**). The sensitivity of $\eta_{Synthesis}$ to influent coexisting anions highlights that to improve the adaptability of EDNR to treat a wide range of wastewaters, future efforts should develop NO_3^--selective AEMs that enable targeted separation of NO_3^- from complex influent matrices.

In contrast to the composition-specific $\eta_{Synthesis}$, $\eta_{Recovery}$ exhibited a generalizable trend with respect to the initial NH_4^+ transference number in the influent (**Fig. 2c, open symbols**). With a

higher coexisting cation concentration, the NH_4^+ ED current efficiency decreased along with its transference number (**Fig. S21**). Experimentally, we observed that the end-of-run $\eta_{Recovery}$ nearly monotonically decreased with decreasing NH_4^+ transference number: 0.84 in baseline simulated wastewater, 0.59 in NO_3^--laden, 0.41 in SO_4^{2-}-laden, and 0.37 in Cl^--laden scenarios. Therefore, to restore nearly complete NH_3 recovery in the presence of coexisting cations, we could extend ED stage duration (pass more charge) or increase ED state electrolyte flow rate (intensify the ED mass transport).

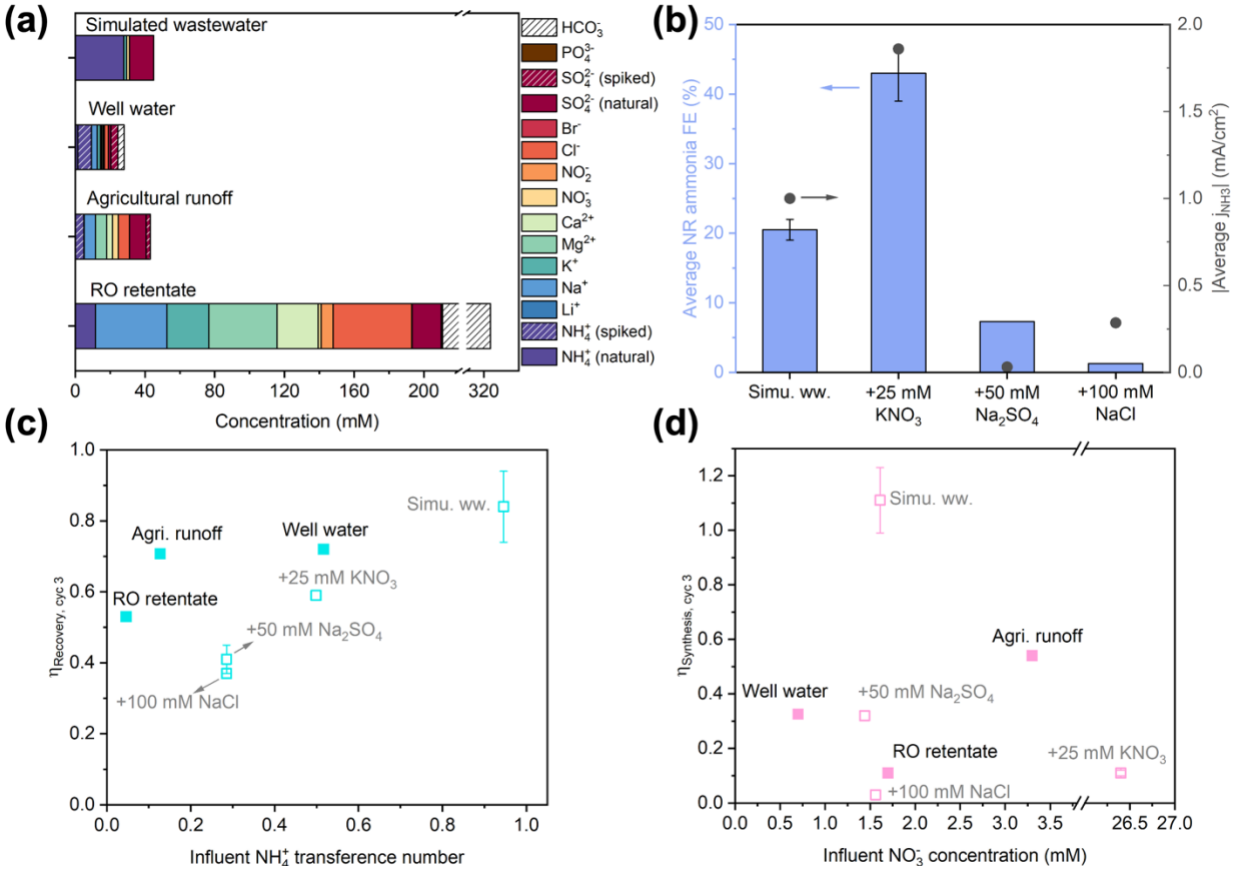

Fig. 2 (a) Compositions of different wastewaters used as influents in EDNR experiments. **(b)** Effects of influent compositions on average NH_3 Faradaic efficiency (left y-axis) and NH_3 partial current density (right

y-axis) in NR stages. Influents: simulated wastewater (13.9 mM $(NH_4)_2SO_4$ + 1.6 mM KNO_3), and simulated wastewater +25 mM KNO_3 (NO_3^--laden), or +50 mM Na_2SO_4 (SO_4^{2-}-laden), or +100 mM NaCl (Cl^--laden). **(c)** End-of-run NH_3 recovery efficiency as a function of influent NH_4^+ transference number, and **(d)** end-of-run NH_3 synthesis efficiency as a function of influent NO_3^- concentration in EDNR experiments using different modified simulated (open symbols) and real wastewater (filled symbols). Error bars represent ± one standard deviation.

Real wastewaters

In addition to understanding deconvoluted effects of influent compositions in modified simulated wastewaters, we examined EDNR performance in real wastewaters with much more complex compositions. We selected three representative wastewaters that contain dilute Nr levels and a wide range of total charge concentrations as the EDNR influent (well water, agricultural runoff, and RO retentate, **Fig. 2a**). To test both ED and NR performances in these real wastewater matrices, we manually added NH_4^+ in the form of $(NH_4)_2SO_4$ to reach a concentration of 8 mM in well water and 4.8 mM in agricultural runoff, ensuring the coexistence of NH_4^+ and NO_3^-. Depending on sampling sites (e.g., livestock farms) and time (e.g., nitrification progress in soil, time since previous rainfall), agricultural runoff could contain a similar level of NH_4^+.[53] For ED performance, we found that the empirical relationship between end-of-run $\eta_{Recovery}$ and initial influent NH_4^+ transference number held very well (**Fig. 2c, filled symbols**). In real wastewater EDNR influents, due to competition from coexisting cations, NH_4^+ ED current efficiency decreased (**Fig. S22**), and $\eta_{Recovery}$ for all three real wastewaters fell short of optimized NR. But notably, in the low NH_4^+ transference number range, real wastewaters outperformed modified simulated wastewaters, suggesting that the CEM is more selective towards monovalent NH_4^+ over divalent cations (Ca^{2+},

371 Mg^{2+}) present in these real wastewaters under our ED operating conditions. Based on **Fig. 2c**, NH_4^+
372 transference in the feedstock with corrections based on divalent cation concentration could be used
373 to predict NH_3 recovery performance in EDNR.

374

375 For NR performance, end-of-run $\eta_{Synthesis}$ in all three wastewaters was far below that of the
376 baseline simulated wastewater and did not correlate with influent NO_3^- concentration (**Fig. 2d**).
377 j_{total} in RO retentate was similar to in the baseline simulated wastewater, but significantly lower in
378 well water and agricultural runoff (**Fig. S23a**). Based on the influent composition effects observed
379 in modified simulated wastewaters, we attributed the cause of impaired NR to unique compositions
380 of each wastewater. RO retentate contains comparable concentrations of NO_3^- and SO_4^{2-} to
381 simulated wastewater, with additional NO_2^- (6.9 mM), Cl^- (45.2 mM), and HCO_3^- (estimated 113.3
382 mM). While NO_2^- could also be reduced and produce NH_3 during NR, it was counterbalanced by
383 adverse effects from Cl^- and possibly HCO_3^- (competitive adsorption,[54,55] electrochemical
384 deprotonation,[56] or electrode surface scaling with divalent cations[49]), leading to significantly lower
385 j_{NH_3} (*ca.* 50% of optimized NR). Well water contains about half as much NO_3^- as simulated
386 wastewater (0.7 *vs.* 1.6 mM), leading to lower j_{NH_3} (15–33% of optimized NR). In contrast,
387 agricultural runoff contains the highest NO_3^- concentration (3.3 mM) among the real wastewaters
388 tested and exhibited higher FE_{NH_3} (45–63%) and similar j_{NH_3} compared to simulated wastewater
389 (**Fig. S23b–d**). Therefore, to compensate for the coexisting cations and elevated NO_3^-
390 concentration in agricultural runoff, we increased the number of EDNR operation to 4 cycles and
391 acquired end-of-run $\eta_{Recovery}$ (>0.77) and $\eta_{Synthesis}$ (>0.70, **Fig. S24**) that approached values in
392 simulated wastewater. Achieving similar efficiencies in real wastewater compared to simulated

wastewater shows the significance of EDNR for accelerating wastewater valorization: employing reactive separations based on systematic studies of electrolyte and operating parameters to understand and mitigate the effects of complex wastewater feedstock compositions.

Long-term EDNR and product purification to treat agricultural runoff

Despite being crucial to implementation, long-term studies conducted under realistic operating conditions are rarely reported for electrochemical Nr recovery processes.[50] Similarly, energy consumption is not always reported in the literature but highly desired by practitioners.[57] Thus, we examined the long-term stability and energy consumption of the EDNR unit process in treating real wastewater. We selected NH_4^+-enriched agricultural runoff as the target feedstock because among the wastewaters we tested, it exhibits moderate Nr concentration, moderate total ionic concentration, and diverse ionic species. Applying operating parameters slightly altered from optimized NR (detailed in **SI Section S3.4**), we conducted 4-cycle EDNR experiments that processed 50 mL of fresh influent per batch (i.e., every 4 EDNR cycles). To demonstrate generation of pure wastewater-derived NH_3 products, we coupled the EDNR process with membrane stripping and formed a near-neutral ammonia phosphate fertilizer solution. The integrated process was conducted for 5 consecutive days and processed a total of 250 mL NH_4^+-enriched agricultural runoff (experimental protocols in **SI Section S1.4**).

The EDNR process demonstrated exceptional long-term robustness. Despite the complex composition of agricultural runoff, end-of-batch NH_3 recovery and synthesis efficiencies approached values achieved in baseline simulated wastewater (0.77 $\pm$0.11 for $\eta_{Recovery}$, 0.66$\pm$0.10

for $\eta_{Synthesis}$) and did not show appreciable decay with extended operation (**Fig. 3a-b**, except for batch 3). NH_4^+ and NO_3^- ED current efficiencies remained steady over time and unimpaired by observed membrane fouling (**Fig. S25–26**), corroborating our conclusion that Nr ionic fluxes were controlled by transport from the influent to membranes. The steady ED performance repeatedly created favorable electrolyte environments for NR, as evidenced by nearly overlapping trends of pH and Nr ion movements across all batches (**Fig. S27–29**). High activity and selectivity were maintained during NR (**Fig. S30**), with total current density at *ca.* 2 mA/cm^2 and FE_{NH_3} >40% across all batches. Within each batch, the FE_{NH_3} in cycle 4 (final cycle) was the lowest due to the low NO_3^- concentrations and loss of volatile NH_3 from the alkaline electrolyte. Starting from the second batch, FE_{NH_3} in cycle 1–3 increased to >60%. In contrast to the more commonly observed losses in electrode activity and selectivity over time, the Ti electrode exhibited an 'activated' NH_3 selectivity induced by the first batch of EDNR (8 hr total in NR) and overnight air exposure (10 hr exposed in an empty cell open to air). Based on our previous study, the near-surface of the Ti electrode in contact with the electrolyte likely converted to TiH_2 after the first EDNR batch; however, TiH_2 exhibits similar nitrate reduction activity and selectivity to unamended Ti.[39] Therefore, we hypothesized that increased NH_3 selectivity arose from altered surface morphology[58–60] or partially oxidized TiH_2/Ti.[61–63] To summarize long-term performance, ED and NR stages showed excellent resilience to real wastewater over extended operation, achieving stable, high NH_3 recovery and synthesis that enable future scale-up.

To extract and concentrate EDNR-recovered and synthesized NH_3 from background electrolytes, we combined EDNR with a low-energy passive separation process, membrane stripping, to recover a single NH_3 product stream. After 5 batches, the acid trap chamber recovered 101 mM NH_3 as a

mixture of $NH_4H_2PO_4$ and $(NH_4)_2HPO_4$ (pH 6.42), which can be directly applied as a fertilizer (mono- and di-ammonium phosphate, MAP and DAP fertilizers, typical application concentration 43–454 mM NH_4^+).[64,65]. Importantly, this combined solution was 12.3 times more concentrated than the influent (8.2 mM total Nr, **Fig. 3c**). Note that this up-concentration factor can be further increased by using (1) a higher volume ratio of influent to NH_3 synthesis/recovery chamber background electrolyte, (2) a higher volume ratio of NH_3 synthesis/recovery chamber background electrolyte to acid trap, or (3) more batches of EDNR operation. This wastewater-derived NH_3 solution exhibits metal cation levels (Na, Mg, K, Ca, Cu) below 10 ppb on inductively coupled plasma optical emission spectroscopy (ICP-OES). From 250 mL agricultural runoff that contains dilute and unusable level of Nr, we recovered a concentrated fertilizer solution that can serve 50 cm^2 of vegetative stage crops, highlighting the suitability of EDNR for decentralized nutrient recovery.

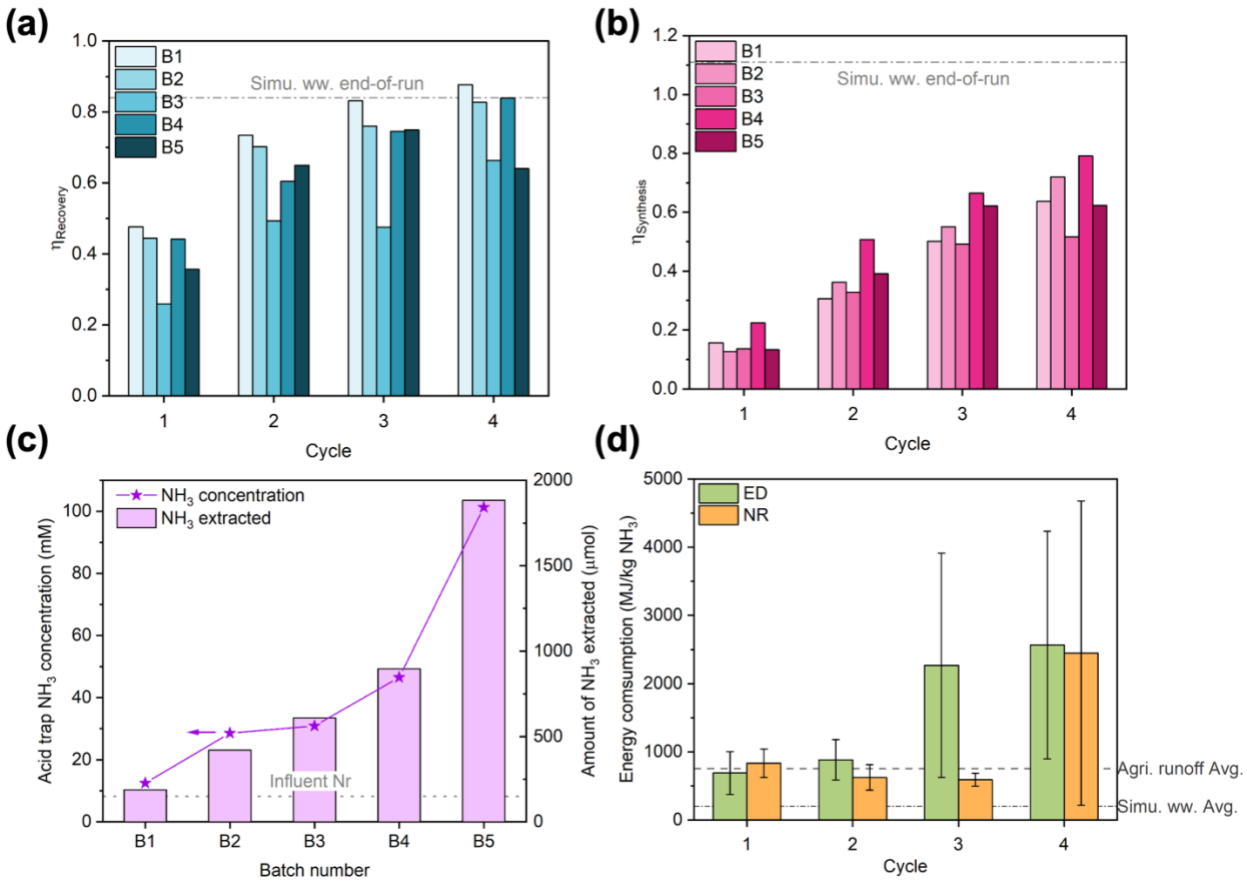

452

453 **Fig. 3** Long-term EDNR using agricultural runoff. **(a)** NH_3 recovery efficiency and **(b)** NH_3 synthesis
454 efficiency in long-term EDNR experiments using agricultural runoff. The few instances where efficiencies
455 decreased with increasing cycle number in B3 and B5 were caused by decreasing NH_3 concentration in
456 corresponding chambers, possibly due to NH_3 evaporation. Dash-dot lines represent the average end-of-run
457 NH_3 recovery and synthesis efficiencies in simulated wastewater feedstock. **(c)** Concentration (left y-axis)
458 and total amount (right y-axis) of NH_3 extracted into the acid trap through membrane stripping. Dotted line
459 represents total Nr concentration in NH_4^+-enriched agricultural runoff influent. **(d)** Energy consumption in
460 NH_3 recovery and synthesis. Large error bars in cycle 3 and cycle 4 resulted from negative NH_3
461 recovery/synthesis in B3 and B5. Because pumping energy typically contributes minimally to the overall
462 energy consumption for electrochemical wastewater treatment processes(<5%[31,34]), we based our
463 calculations solely on electrical energy consumed in the EDNR process. Error bars represent ± one standard

deviation. Dash and dash-dot lines represent the average energy consumption for NH_3 production in NH_4^+-enriched agricultural runoff and simulated wastewater feedstocks, respectively.

To inform distributed NH_3 manufacturing from wastewaters, we evaluated EDNR energy consumption and identified opportunities for future improvements (**Fig. 3d**). In the first two cycles, ED and NR stages consumed similar amounts of energy per kg NH_3 produced. Starting from cycle 3, much more energy was consumed in ED to recover the marginal amount of residual influent NH_4^+ due to the significantly lower current efficiency (**Fig. S26a**). NR energy consumption only increased in the last cycle (**Fig. 3d**) due to the low cycle 4 FE_{NH_3} (**Fig. S30b**). Accounting for both ED and NR stages, the average energy consumption using the NH_4^+-enriched agricultural runoff was 920 MJ/kg-N. In comparison, the average energy consumption in simulated wastewater was 245 MJ/kg-N (**Fig. S31a**). We attributed the 3.75 times higher energy consumption in real wastewater to its significantly lower NH_4^+ concentration (5 times lower) and CEM scaling caused by divalent cations (leading to higher cell voltage, **Fig. S31b**). These energy consumption values are among those for state-of-the-art electrochemical NH_3 manufacturing technologies using similarly dilute Nr feedstocks (**Table S6**). But distinct from most literature reports, the feedstock used in this work was a complex real wastewater with dilute Nr (*vs.* simplistic electrolytes with concentrated Nr), and a purified product stream was recovered with very low energy input (*vs.* products not separated from the influent or requiring downstream energy/chemical-intensive separation). Although the EDNR energy consumption is several times higher than traditional wastewater Nr removal (e.g., nitrification/denitrification, Anammox; 10–100 MJ/kg N)[12,66] and NH_3 manufacturing technologies (e.g., Haber–Bosch, 31.6 MJ/kg N)[50], this electrochemical reactive separation unit process enables highly tunable and robust wastewater refining at the point

of wastewater generation. It can operate independently or as a downstream module in a treatment train to extract residual dilute Nr (e.g., after electrochemical stripping using urine feedstock[50]). Future work can reduce the energy consumption by: (1) reducing the number of cycles to avoid operating in low mass transport driving force regions, when near-complete removal and recovery are not required; (2) employing more active ED and NR electrodes to lower overpotential; and (3) adding antifoulants or other mitigation strategies into the NH_3 recovery chamber to prevent CEM fouling.

CONCLUSIONS

This study demonstrated that Electrodialysis and Nitrate Reduction (EDNR) is a highly tunable and robust reaction separation process to recover and synthesize NH_3 from dilute, Nr-polluted wastewaters. We found that engineering the NR reaction environment via electrochemical separations (electrolyte compositions and applied potential) plays a crucial role in improving electrocatalytic NH_3 synthesis. In wastewater feedstocks, NH_4^+ transference number largely determines the NH_3 recovery efficiency, while NO_3^- concentration as well as coexisting anion identity and concentration together influence the NH_3 synthesis efficiency. Due to their complex compositions, real wastewaters tested in this study generally exhibited lower efficiency and higher energy consumption compared to simulated wastewater. Demonstrated using generic electrode and membrane materials here, the EDNR reactor can be used as a platform to benchmark high-performance materials tailored to feedstock conditions. Development of more active NR electrodes, monovalent-selective CEM, NO_3^--selective AEM, and engineering strategies will advance the EDNR process to become more energy-efficient and compatible with an even wider range of feedstocks. Shown as a prototype here, EDNR can remediate impaired feedstocks and valorize Nr

pollutants in a distributed manner. The process has great viability in scenarios not served by conventional manufacturing (farms, remote communities), and regions like sub-Saharan Africa,[67] where limited access to centralized infrastructure and raw chemical inputs inhibits access to clean water and fertilizer. These issues of scale and access extend beyond the context of Nr recovery, which underscores the potential utility of EDNR as a modular architecture that enables wastewater refining by leveraging reactive separation and valorization of other ionic pollutants in wastewater (e.g., sulfide oxidation, sulfate reduction). Our future efforts will focus on assessing the technoeconomic viability of the EDNR process and advancing the scale and TRL of the process for realistic scenarios as an endeavor to circularize the nitrogen cycle and sustain chemical manufacturing for future generations.

ACKNOWLEDGEMENTS

We are grateful to several funders of this work. J. G. acknowledges the National Science Foundation EFRI program (Award 2132007) and the Chemical Engineering Department at Stanford University. M.J.L. acknowledges support from the National Aeronautics and Space Administration (NASA) Space Technology Graduate Research Opportunities fellowship (Award 80NSSC20K1207) and Northern California Chapter of the ARCS Foundation (Rhoda Goldman Memorial Scholarship). D. M. M. acknowledges support from the National Aeronautics and Space Administration (NASA) Space Technology Graduate Research Opportunities fellowship (Award 80NSSC22K1191). K. S. W. acknowledges the Sustainability Accelerator within the Doerr School of Sustainability at Stanford University. The authors thank Silicon Valley Clean Water for providing wastewater samples; Ouriel Ndalamba and Kristy Chan for support on conducting

experiments; and the Tarpeh, Jaramillo, Maher, Mauter, and Lobell groups for critical feedback on the project.

SUPPORTING INFORMATION

Experimental details; supporting tables; and additional experimental and simulation data.

REFERENCES

(1) *Science for Environmental Protection: The Road Ahead*; National Academies Press: Washington, D.C., 2012. https://doi.org/10.17226/13510.
(2) MacFarlane, D. R.; Cherepanov, P. V.; Choi, J.; Suryanto, B. H. R.; Hodgetts, R. Y.; Bakker, J. M.; Ferrero Vallana, F. M.; Simonov, A. N. A Roadmap to the Ammonia Economy. *Joule* **2020**, *4* (6), 1186–1205. https://doi.org/10.1016/j.joule.2020.04.004.
(3) Lim, J.; Fernández, C. A.; Lee, S. W.; Hatzell, M. C. Ammonia and Nitric Acid Demands for Fertilizer Use in 2050. *ACS Energy Lett.* **2021**, *6* (10), 3676–3685. https://doi.org/10.1021/acsenergylett.1c01614.
(4) Galloway, J. N.; Cowling, E. B. Reactive Nitrogen and The World: 200 Years of Change. *ambi* **2002**, *31* (2), 64–71. https://doi.org/10.1579/0044-7447-31.2.64.
(5) Chen, J. G.; Crooks, R. M.; Seefeldt, L. C.; Bren, K. L.; Bullock, R. M.; Darensbourg, M. Y.; Holland, P. L.; Hoffman, B.; Janik, M. J.; Jones, A. K.; Kanatzidis, M. G.; King, P.; Lancaster, K. M.; Lymar, S. V.; Pfromm, P.; Schneider, W. F.; Schrock, R. R. Beyond Fossil Fuel–Driven Nitrogen Transformations. *Science* **2018**, *360* (6391), eaar6611. https://doi.org/10.1126/science.aar6611.
(6) Steffen, W.; Richardson, K.; Rockström, J.; Cornell, S. E.; Fetzer, I.; Bennett, E. M.; Biggs, R.; Carpenter, S. R.; de Vries, W.; de Wit, C. A.; Folke, C.; Gerten, D.; Heinke, J.; Mace, G. M.; Persson, L. M.; Ramanathan, V.; Reyers, B.; Sörlin, S. Planetary Boundaries: Guiding Human Development on a Changing Planet. *Science* **2015**, *347* (6223), 1259855. https://doi.org/10.1126/science.1259855.
(7) Bodirsky, B. L.; Popp, A.; Lotze-Campen, H.; Dietrich, J. P.; Rolinski, S.; Weindl, I.; Schmitz, C.; Müller, C.; Bonsch, M.; Humpenöder, F.; Biewald, A.; Stevanovic, M. Reactive Nitrogen Requirements to Feed the World in 2050 and Potential to Mitigate Nitrogen Pollution. *Nat Commun* **2014**, *5* (1), 3858. https://doi.org/10.1038/ncomms4858.
(8) Miller, D. M.; Abels, K.; Guo, J.; Williams, K. S.; Liu, M. J.; Tarpeh, W. A. Electrochemical Wastewater Refining: A Vision for Circular Chemical Manufacturing. *J. Am. Chem. Soc.* **2023**, *145* (36), 19422–19439. https://doi.org/10.1021/jacs.3c01142.

(9) Garcia-Segura, S.; Lanzarini-Lopes, M.; Hristovski, K.; Westerhoff, P. Electrocatalytic Reduction of Nitrate: Fundamentals to Full-Scale Water Treatment Applications. *Applied Catalysis B: Environmental* **2018**, *236*, 546–568. https://doi.org/10.1016/j.apcatb.2018.05.041.
(10) Hansen, B.; Thorling, L.; Schullehner, J.; Termansen, M.; Dalgaard, T. Groundwater Nitrate Response to Sustainable Nitrogen Management. *Sci Rep* **2017**, *7* (1), 8566. https://doi.org/10.1038/s41598-017-07147-2.
(11) Abascal, E.; Gómez-Coma, L.; Ortiz, I.; Ortiz, A. Global Diagnosis of Nitrate Pollution in Groundwater and Review of Removal Technologies. *Science of The Total Environment* **2022**, *810*, 152233. https://doi.org/10.1016/j.scitotenv.2021.152233.
(12) Theerthagiri, J.; Park, J.; Das, H. T.; Rahamathulla, N.; Cardoso, E. S. F.; Murthy, A. P.; Maia, G.; Vo, D. N.; Choi, M. Y. Electrocatalytic Conversion of Nitrate Waste into Ammonia: A Review. *Environ Chem Lett* **2022**, *20* (5), 2929–2949. https://doi.org/10.1007/s10311-022-01469-y.
(13) Niemann, V. A.; Benedek, P.; Guo, J.; Xu, Y.; Blair, S. J.; Corson, E. R.; Nielander, A. C.; Jaramillo, T. F.; Tarpeh, W. A. Co-Designing Electrocatalytic Systems with Separations To Improve the Sustainability of Reactive Nitrogen Management. *ACS Catal.* **2023**, *13* (9), 6268–6279. https://doi.org/10.1021/acscatal.3c00933.
(14) Tarpeh, W. A.; Chen, X. Making Wastewater Obsolete: Selective Separations to Enable Circular Water Treatment. *Environmental Science and Ecotechnology* **2021**, *5*, 100078. https://doi.org/10.1016/j.ese.2021.100078.
(15) Zito, A. M.; Clarke, L. E.; Barlow, J. M.; Bím, D.; Zhang, Z.; Ripley, K. M.; Li, C. J.; Kummeth, A.; Leonard, M. E.; Alexandrova, A. N.; Brushett, F. R.; Yang, J. Y. Electrochemical Carbon Dioxide Capture and Concentration. *Chem. Rev.* **2023**, *123* (13), 8069–8098. https://doi.org/10.1021/acs.chemrev.2c00681.
(16) Freyman, M. C.; Huang, Z.; Ravikumar, D.; Duoss, E. B.; Li, Y.; Baker, S. E.; Pang, S. H.; Schaidle, J. A. Reactive CO2 Capture: A Path Forward for Process Integration in Carbon Management. *Joule* **2023**, *7* (4), 631–651. https://doi.org/10.1016/j.joule.2023.03.013.
(17) Siegel, R. E.; Pattanayak, S.; Berben, L. A. Reactive Capture of CO2: Opportunities and Challenges. *ACS Catal.* **2023**, *13* (1), 766–784. https://doi.org/10.1021/acscatal.2c05019.
(18) Gadikota, G. Multiphase Carbon Mineralization for the Reactive Separation of CO2 and Directed Synthesis of H2. *Nat Rev Chem* **2020**, *4* (2), 78–89. https://doi.org/10.1038/s41570-019-0158-3.
(19) Sanz-Pérez, E. S.; Murdock, C. R.; Didas, S. A.; Jones, C. W. Direct Capture of CO2 from Ambient Air. *Chem. Rev.* **2016**, *116* (19), 11840–11876. https://doi.org/10.1021/acs.chemrev.6b00173.
(20) Dutta, P. K.; Rabaey, K.; Yuan, Z.; Rozendal, R. A.; Keller, J. Electrochemical Sulfide Removal and Recovery from Paper Mill Anaerobic Treatment Effluent. *Water Research* **2010**, *44* (8), 2563–2571. https://doi.org/10.1016/j.watres.2010.01.008.
(21) Jangam, K.; Chen, Y.-Y.; Qin, L.; Fan, L.-S. Perspectives on Reactive Separation and Removal of Hydrogen Sulfide. *Chemical Engineering Science: X* **2021**, *11*, 100105. https://doi.org/10.1016/j.cesx.2021.100105.
(22) Blázquez, E.; Gabriel, D.; Baeza, J. A.; Guisasola, A.; Freguia, S.; Ledezma, P. Recovery of Elemental Sulfur with a Novel Integrated Bioelectrochemical System with an Electrochemical Cell. *Science of The Total Environment* **2019**, *677*, 175–183. https://doi.org/10.1016/j.scitotenv.2019.04.406.

(23) Zhai, L.-F.; Song, W.; Tong, Z.-H.; Sun, M. A Fuel-Cell-Assisted Iron Redox Process for Simultaneous Sulfur Recovery and Electricity Production from Synthetic Sulfide Wastewater. *Journal of Hazardous Materials* **2012**, *243*, 350–356. https://doi.org/10.1016/j.jhazmat.2012.10.046.
(24) Sergienko, N.; Radjenovic, J. Manganese Oxide-Based Porous Electrodes for Rapid and Selective (Electro)Catalytic Removal and Recovery of Sulfide from Wastewater. *Applied Catalysis B: Environmental* **2020**, *267*, 118608. https://doi.org/10.1016/j.apcatb.2020.118608.
(25) Wu, L.; Zhang, C.; Kim, S.; Hatton, T. A.; Mo, H.; Waite, T. D. Lithium Recovery Using Electrochemical Technologies: Advances and Challenges. *Water Research* **2022**, *221*, 118822. https://doi.org/10.1016/j.watres.2022.118822.
(26) Luo, G.; Li, X.; Chen, L.; Chao, Y.; Zhu, W. Electrochemical Lithium Ion Pumps for Lithium Recovery: A Systematic Review and Influencing Factors Analysis. *Desalination* **2023**, *548*, 116228. https://doi.org/10.1016/j.desal.2022.116228.
(27) Liu, G.; Zhao, Z.; He, L. Highly Selective Lithium Recovery from High Mg/Li Ratio Brines. *Desalination* **2020**, *474*, 114185. https://doi.org/10.1016/j.desal.2019.114185.
(28) Yang, S.; Zhang, F.; Ding, H.; He, P.; Zhou, H. Lithium Metal Extraction from Seawater. *Joule* **2018**, *2* (9), 1648–1651. https://doi.org/10.1016/j.joule.2018.07.006.
(29) Yu, J.; Fang, D.; Zhang, H.; Leong, Z. Y.; Zhang, J.; Li, X.; Yang, H. Y. Ocean Mining: A Fluidic Electrochemical Route for Lithium Extraction from Seawater. *ACS Materials Lett.* **2020**, *2* (12), 1662–1668. https://doi.org/10.1021/acsmaterialslett.0c00385.
(30) Zhao, Z.; Liu, G.; Jia, H.; He, L. Sandwiched Liquid-Membrane Electrodialysis: Lithium Selective Recovery from Salt Lake Brines with High Mg/Li Ratio. *Journal of Membrane Science* **2020**, *596*, 117685. https://doi.org/10.1016/j.memsci.2019.117685.
(31) Tarpeh, W. A.; Barazesh, J. M.; Cath, T. Y.; Nelson, K. L. Electrochemical Stripping to Recover Nitrogen from Source-Separated Urine. *Environ. Sci. Technol.* **2018**, *52* (3), 1453–1460. https://doi.org/10.1021/acs.est.7b05488.
(32) Ferrari, F.; Pijuan, M.; Molenaar, S.; Duinslaeger, N.; Sleutels, T.; Kuntke, P.; Radjenovic, J. Ammonia Recovery from Anaerobic Digester Centrate Using Onsite Pilot Scale Bipolar Membrane Electrodialysis Coupled to Membrane Stripping. *Water Research* **2022**, *218*, 118504. https://doi.org/10.1016/j.watres.2022.118504.
(33) Dong, H.; Laguna, C. M.; Liu, M. J.; Guo, J.; Tarpeh, W. A. Electrified Ion Exchange Enabled by Water Dissociation in Bipolar Membranes for Nitrogen Recovery from Source-Separated Urine. *Environ. Sci. Technol.* **2022**, *56* (22), 16134–16143. https://doi.org/10.1021/acs.est.2c03771.
(34) Sun, J.; Garg, S.; Waite, T. D. A Novel Integrated Flow-Electrode Capacitive Deionization and Flow Cathode System for Nitrate Removal and Ammonia Generation from Simulated Groundwater. *Environ. Sci. Technol.* **2023**. https://doi.org/10.1021/acs.est.3c03922.
(35) Kim, K.; Zagalskaya, A.; Ng, J. L.; Hong, J.; Alexandrov, V.; Pham, T. A.; Su, X. Coupling Nitrate Capture with Ammonia Production through Bifunctional Redox-Electrodes. *Nat Commun* **2023**, *14* (1), 823. https://doi.org/10.1038/s41467-023-36318-1.
(36) Gao, J.; Shi, N.; Li, Y.; Jiang, B.; Marhaba, T.; Zhang, W. Electrocatalytic Upcycling of Nitrate Wastewater into an Ammonia Fertilizer via an Electrified Membrane. *Environ. Sci. Technol.* **2022**. https://doi.org/10.1021/acs.est.1c08442.

(37) Liu, M. J.; Miller, D. M.; Tarpeh, W. A. Reactive Separation of Ammonia from Wastewater Nitrate via Molecular Electrocatalysis. *Environ. Sci. Technol. Lett.* **2023**, *10* (5), 458–463. https://doi.org/10.1021/acs.estlett.3c00205.
(38) McEnaney, J. M.; Blair, S. J.; Nielander, A. C.; Schwalbe, J. A.; Koshy, D. M.; Cargnello, M.; Jaramillo, T. F. Electrolyte Engineering for Efficient Electrochemical Nitrate Reduction to Ammonia on a Titanium Electrode. *ACS Sustainable Chem. Eng.* **2020**, *8* (7), 2672–2681. https://doi.org/10.1021/acssuschemeng.9b05983.
(39) Liu, M. J.; Guo, J.; Hoffman, A. S.; Stenlid, J. H.; Tang, M. T.; Corson, E. R.; Stone, K. H.; Abild-Pedersen, F.; Bare, S. R.; Tarpeh, W. A. Catalytic Performance and Near-Surface X-Ray Characterization of Titanium Hydride Electrodes for the Electrochemical Nitrate Reduction Reaction. *J. Am. Chem. Soc.* **2022**, *144* (13), 5739–5744. https://doi.org/10.1021/jacs.2c01274.
(40) Guo, J.; Brimley, P.; Liu, M. J.; Corson, E. R.; Muñoz, C.; Smith, W. A.; Tarpeh, W. A. Mass Transport Modifies the Interfacial Electrolyte to Influence Electrochemical Nitrate Reduction. *ACS Sustainable Chem. Eng.* **2023**, *11* (20), 7882–7893. https://doi.org/10.1021/acssuschemeng.3c01057.
(41) Deng, B.; Huang, M.; Zhao, X.; Mou, S.; Dong, F. Interfacial Electrolyte Effects on Electrocatalytic CO2 Reduction. *ACS Catal.* **2022**, *12* (1), 331–362. https://doi.org/10.1021/acscatal.1c03501.
(42) Bui, J. C.; Kim, C.; King, A. J.; Romiluyi, O.; Kusoglu, A.; Weber, A. Z.; Bell, A. T. Engineering Catalyst–Electrolyte Microenvironments to Optimize the Activity and Selectivity for the Electrochemical Reduction of CO2 on Cu and Ag. *Acc. Chem. Res.* **2022**, *55* (4), 484–494. https://doi.org/10.1021/acs.accounts.1c00650.
(43) Ruggiero, B. N.; Sanroman Gutierrez, K. M.; George, J. D.; Mangan, N. M.; Notestein, J. M.; Seitz, L. C. Probing the Relationship between Bulk and Local Environments to Understand Impacts on Electrocatalytic Oxygen Reduction Reaction. *Journal of Catalysis* **2022**, *414*, 33–43. https://doi.org/10.1016/j.jcat.2022.08.025.
(44) Kastlunger, G.; Wang, L.; Govindarajan, N.; Heenen, H. H.; Ringe, S.; Jaramillo, T.; Hahn, C.; Chan, K. Using pH Dependence for Understanding Mechanisms in Electrochemical CO Reduction. **2021**. https://doi.org/10.33774/chemrxiv-2021-jn28g.
(45) Hu, Q.; Yang, K.; Peng, O.; Li, M.; Ma, L.; Huang, S.; Du, Y.; Xu, Z.-X.; Wang, Q.; Chen, Z.; Yang, M.; Loh, K. P. Ammonia Electrosynthesis from Nitrate Using a Ruthenium–Copper Cocatalyst System: A Full Concentration Range Study. *J. Am. Chem. Soc.* **2023**. https://doi.org/10.1021/jacs.3c10516.
(46) Dima, G. E.; de Vooys, A. C. A.; Koper, M. T. M. Electrocatalytic Reduction of Nitrate at Low Concentration on Coinage and Transition-Metal Electrodes in Acid Solutions. *Journal of Electroanalytical Chemistry* **2003**, *554–555*, 15–23. https://doi.org/10.1016/S0022-0728(02)01443-2.
(47) Horányi, G.; Rizmayer, E. M. Role of Adsorption Phenomena in the Electrocatalytic Reduction of Nitric Acid at a Platinized Platinum Electrode. *Journal of Electroanalytical Chemistry and Interfacial Electrochemistry* **1982**, *140* (2), 347–366. https://doi.org/10.1016/0022-0728(82)85178-4.
(48) Alkhadra, M. A.; Su, X.; Suss, M. E.; Tian, H.; Guyes, E. N.; Shocron, A. N.; Conforti, K. M.; de Souza, J. P.; Kim, N.; Tedesco, M.; Khoiruddin, K.; Wenten, I. G.; Santiago, J. G.; Hatton, T. A.; Bazant, M. Z. Electrochemical Methods for Water Purification, Ion

Separations, and Energy Conversion. *Chem. Rev.* **2022**, *122* (16), 13547–13635. https://doi.org/10.1021/acs.chemrev.1c00396.
(49) Atrashkevich, A.; Fajardo, A. S.; Westerhoff, P.; Walker, W. S.; Sánchez-Sánchez, C. M.; Garcia-Segura, S. Overcoming Barriers for Nitrate Electrochemical Reduction: By-Passing Water Hardness. *Water Research* **2022**, *225*, 119118. https://doi.org/10.1016/j.watres.2022.119118.
(50) Kogler, A.; Sharma, N.; Tiburcio, D.; Gong, M.; Miller, D. M.; Williams, K. S.; Chen, X.; Tarpeh, W. A. Long-Term Robustness and Failure Mechanisms of Electrochemical Stripping for Wastewater Ammonia Recovery. *ACS Environ. Au* **2024**. https://doi.org/10.1021/acsenvironau.3c00058.
(51) Miller, D.; Abels, K.; Guo, J.; Williams, K.; Liu, M.; Tarpeh, W. Electrochemical Wastewater Refining: A Vision for Circular Chemical Manufacturing. ChemRxiv April 5, 2023. https://doi.org/10.26434/chemrxiv-2023-1tdxx.
(52) Carvalho, O. Q.; Marks, R.; Nguyen, H. K. K.; Vitale-Sullivan, M. E.; Martinez, S. C.; Árnadóttir, L.; Stoerzinger, K. A. Role of Electronic Structure on Nitrate Reduction to Ammonium: A Periodic Journey. *J. Am. Chem. Soc.* **2022**, *144* (32), 14809–14818. https://doi.org/10.1021/jacs.2c05673.
(53) de Vries, W.; Kros, J.; Voogd, J. C.; Ros, G. H. Integrated Assessment of Agricultural Practices on Large Scale Losses of Ammonia, Greenhouse Gases, Nutrients and Heavy Metals to Air and Water. *Science of The Total Environment* **2023**, *857*, 159220. https://doi.org/10.1016/j.scitotenv.2022.159220.
(54) Makover, J.; Hasson, D.; Semiat, R.; Shemer, H. Electrochemical Removal of Nitrate from High Salinity Waste Stream in a Continuous Flow Reactor. *Journal of Environmental Chemical Engineering* **2020**, *8* (3), 103727. https://doi.org/10.1016/j.jece.2020.103727.
(55) Huang, W.; Li, M.; Zhang, B.; Feng, C.; Lei, X.; Xu, B. Influence of Operating Conditions on Electrochemical Reduction of Nitrate in Groundwater. *Water Environment Research* **2013**, *85* (3), 224–231. https://doi.org/10.2175/106143012X13418552642047.
(56) Marcandalli, G.; Boterman, K.; Koper, M. T. M. Understanding Hydrogen Evolution Reaction in Bicarbonate Buffer. *Journal of Catalysis* **2022**, *405*, 346–354. https://doi.org/10.1016/j.jcat.2021.12.012.
(57) Kogler, A.; Farmer, M.; Simon, J. A.; Tilmans, S.; Wells, G. F.; Tarpeh, W. A. Systematic Evaluation of Emerging Wastewater Nutrient Removal and Recovery Technologies to Inform Practice and Advance Resource Efficiency. *ACS EST Eng.* **2021**, *1* (4), 662–684. https://doi.org/10.1021/acsestengg.0c00253.
(58) Krzywda, P. M.; Rodríguez, A. P.; Cino, L.; Benes, N. E.; Mei, B. T.; Mul, G. Electroreduction of NO3− on Tubular Porous Ti Electrodes. *Catal. Sci. Technol.* **2022**, *12* (10), 3281–3288. https://doi.org/10.1039/D2CY00289B.
(59) Lim, J.; Liu, C.-Y.; Park, J.; Liu, Y.-H.; Senftle, T. P.; Lee, S. W.; Hatzell, M. C. Structure Sensitivity of Pd Facets for Enhanced Electrochemical Nitrate Reduction to Ammonia. *ACS Catal.* **2021**, *11* (12), 7568–7577. https://doi.org/10.1021/acscatal.1c01413.
(60) Su, J. F.; Kuan, W.-F.; Liu, H.; Huang, C. P. Mode of Electrochemical Deposition on the Structure and Morphology of Bimetallic Electrodes and Its Effect on Nitrate Reduction toward Nitrogen Selectivity. *Applied Catalysis B: Environmental* **2019**, *257*, 117909. https://doi.org/10.1016/j.apcatb.2019.117909.

(61) Jia, R.; Wang, Y.; Wang, C.; Ling, Y.; Yu, Y.; Zhang, B. Boosting Selective Nitrate Electroreduction to Ammonium by Constructing Oxygen Vacancies in TiO2. *ACS Catal.* **2020**, *10* (6), 3533–3540. https://doi.org/10.1021/acscatal.9b05260.
(62) *Insight into Hydrogenation Selectivity of the Electrocatalytic Nitrate-to-Ammonia Reduction Reaction via Enhancing the Proton Transport - Xu - 2022 - ChemSusChem - Wiley Online Library*. https://chemistry-europe.onlinelibrary.wiley.com/doi/10.1002/cssc.202102450 (accessed 2024-01-30).
(63) Chen, Y.; Yang, C.; Li, H.; Ma, Z.; Wu, D.; Yao, Y.; Shen, X.; Ma, D. Ti3+ Redox Dynamics Enabling Efficient Nitrate Reduction to Ammonia on Ti2O3. *Chemical Engineering Journal* **2024**, *481*, 148857. https://doi.org/10.1016/j.cej.2024.148857.
(64) *soluMAP® - K+S Aktiengesellschaft*. https://www.kpluss.com/en-us/our-business-products/agriculture/products/en-solumap/ (accessed 2024-01-31).
(65) Chowdhury, Md. A. H.; Sultana, T.; Rahman, Md. A.; Chowdhury, T.; Enyoh, C. E.; Saha, B. K.; Qingyue, W. Nitrogen Use Efficiency and Critical Leaf N Concentration of Aloe Vera in Urea and Diammonium Phosphate Amended Soil. *Heliyon* **2020**, *6* (12), e05718. https://doi.org/10.1016/j.heliyon.2020.e05718.
(66) Liu, M. J.; Neo, B. S.; Tarpeh, W. A. Building an Operational Framework for Selective Nitrogen Recovery via Electrochemical Stripping. *Water Research* **2020**, *169*, 115226. https://doi.org/10.1016/j.watres.2019.115226.
(67) Wong, C. A.; Lobell, D. B.; Mauter, M. S. Multicriteria Suitability Index for Prioritizing Early-Stage Deployments of Wastewater-Derived Fertilizers in Sub-Saharan Africa. *Environ. Sci. Technol.* **2023**. https://doi.org/10.1021/acs.est.3c05435.